XV International Conference on Computational Plasticity. Fundamentals and Applications
COMPLAS 2019
E. Oñate, D.R.J. Owen, D. Peric, M. Chiumenti & Eduardo de Souza Neto (Eds)

MODELING ANISOTROPIC AND RATE-DEPENDENT PLASTICITY IN SHORT-FIBER REINFORCED THERMOPLASTICS

AHMAD AMIRI-RAD[*,†], LEONID V. PASTUKHOV[*,†], LEON E. GOVAERT[*] AND JOHANNES A. W. VAN DOMMELEN[*]

[*] Eindhoven University of Technology, P.O. Box 513, 5600 MB, Eindhoven, the Netherlands

[†] Dutch Polymer Institute (DPI), P.O. Box 902, 5600 AX, Eindhoven, the Netherlands

Key words: Short-Fiber Composites, Rate-Dependent Plasticity, Computational Mechanics, Constitutive Modeling

Abstract. In this study, an anisotropic viscoelastic-viscoplastic macro-mechanical model is presented for short-fiber reinforced thermoplastics (SFRT). In injection molding of SFRT, the fiber orientation is influenced by the flow velocity profile which varies throughout the mold. The flow-induced orientation in the microstructure leads to anisotropy in the mechanical response. In addition to the mechanical anisotropy, SFRTs show time dependent behavior because of the thermoplastic matrix. The developed model captures the effects of both material orientation and loading rate on the yield behavior. In this study, uniaxial tests are performed at different strain rates and material orientations with samples cut from injection molded plaques. The experimental results show that the effects of loading rate and material orientation on the yield are decoupled. The presented model takes advantage of this observation to simplify material characterization. An implicit integration scheme is used for the numerical implementation of the model as a UMAT in ABAQUS. Multiple relaxation times are used in order to capture the nonlinear pre-yield regime. An efficient method for obtaining the model parameters for different modes is proposed. Experimental results are used for validation of the model and a good agreement is observed for the prediction of viscoelastic and viscoplastic behavior.

1 INTRODUCTION

Injection-molded short-fiber composites are used for a variety of load-bearing structures, especially in the automotive industry. Their fast and cost-efficient production, light weight and better mechanical properties compared to unfilled plastics are among the reasons for their popularity. In the injection-molding process, the flow causes the fibers to be oriented, which leads to anisotropic mechanical properties. Also, because of the polymer matrix, the mechanical response is time-dependent. This paper aims to propose a reliable and accurate prediction tool for this complex mechanical response.

In this study, a macro-mechanical continuum-based constitutive model is presented for the components based on short-fiber reinforced thermoplastics. This model is built upon the framework of the Eindhoven Glassy Polymer (EGP) model [1–3] which has been successfully used for modeling time-dependent behavior of unfilled polymers. To describe the rate-dependent plasticity this model does not use a classic explicit yield surface and instead treats the polymer as a fluid with a very high initial viscosity which is exponentially reduced with increasing stress. This model belongs to a class of models which follow the pioneering work of Haward and Thackray [4]. Some other examples from this group are the BPA model [5–7] and OGR model [8–10].

The model presented here aims to capture the anisotropic viscoelastic-viscoplastic response of short-fiber composites. To model the rate-dependent and anisotropic yield behavior the associated flow rule proposed by van Erp et al [11] is incorporated into the framework of EGP. This flow rule uses Hill's anisotropic effective stress along with an Eyring type equation. Also, modifications to the EGP model is made to capture the anisotropy in the viscoelastic response. The model is developed based on the observation that the effects of orientation and loading rate on yield stress are factorizable. Experimental results demonstrating this behavior are presented in the following sections.

In the next sections, first, the experimental observations and the developed constitutive model are presented. Next, numerical implementation and material characterization are discussed. In the end, simulations are performed to investigate the performance of the model.

2 CONSTITUTIVE MODEL

The flow-induced fiber orientation causes anisotropy of the mechanical response of injection-molded short-fiber composites. To investigate the dependence of the elastic and yield behavior on the material orientation and strain rate, uniaxial tests at various constant strain rates are performed on specimens cut from injection molded plaques. The material used in this study is SABIC Lexan® 3412R PC (20 wt% short E-glass fiber-reinforced polycarbonate) from SABIC Innovative Plastics, the Netherlands. Figure 1 (a) shows measured values for yield stress at different strain rates and orientations in a double log plot. Angle ϕ shows the angle with respect to the main mold flow direction at which, the specimens are cut. In Figure 1 (b) stress-strain curves for the strain rate of 10^{-4} s^{-1} is shown. As can be seen in these figures, the mechanical response is dependent on the specimen orientation and loading rate. In the double log plot shown in Figure 1 (a), the curves for different angles have the same slope and only a vertical shift is observed as the orientation is changed. This shows the effect of material orientation and strain-rate on the yield behavior are factorizable. van Erp et al. [11] showed their proposed associated flow rule can capture this property. This makes the characterization process simpler since the effects of orientation and loading rate can be taken apart.

In the EGP model, total stress $\boldsymbol{\sigma}$ consists of two components acting in parallel. The components are called driving stress $\boldsymbol{\sigma}_s$ which is the dominant contribution in the pre-yield regime, and the hardening stress $\boldsymbol{\sigma}_r$ which is more important in the post-yield behavior. The mechanical analog of the model is shown in Figure 2. The hardening stress comes

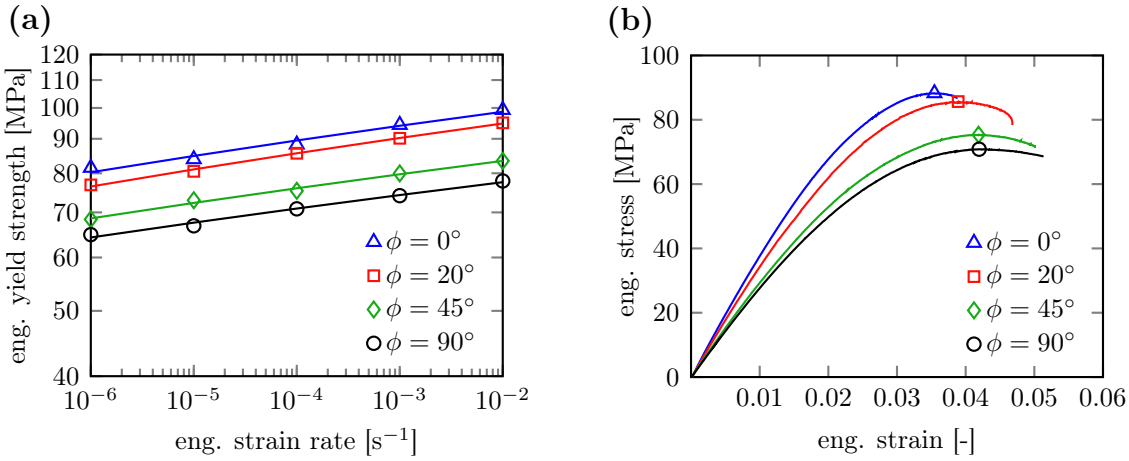

Figure 1: (a) Measured yield stress values at different material orientations and strain rates for polycarbonate with 20 wt% glass fiber; solid lines are guide-to-the-eye (b) stress-strain curves for uniaxial tension tests on polycarbonate with 20 wt% glass fiber at a constant strain rate of 10^{-4} s^{-1} for different material orientations.

from the spring with the modulus G_r and the driving stress is the sum of stress values from all the Maxwell branches. The use of multiple Maxwell branches helps modeling of the nonlinear and rate-dependent pre-yield regime. The total stress is written as:

$$\boldsymbol{\sigma} = \boldsymbol{\sigma}_r + \sum_{i=1}^{n} \boldsymbol{\sigma}_{s,i}, \tag{1}$$

where n is the number of Maxwell elements, $\boldsymbol{\sigma}_{s,i}$ is driving stress component from the ith Maxwell branch and $\boldsymbol{\sigma}_r$ is the hardening stress. The hardening stress is not utilized in the current study since samples fail at relatively low plastic strains. To model the elastic anisotropy, linear orthotropic springs are used in each Maxwell element. To calculate stress in each Maxwell branch, first, a second Piola-Kirchhoff type stress is calculated in the intermediate configuration according to:

$$\hat{\boldsymbol{S}}_{s,i} = {}^4\hat{\boldsymbol{C}}_i : \hat{\boldsymbol{E}}_{e,i}, \tag{2}$$

where $\hat{\boldsymbol{E}}_{e,i}$ shows the Green-Lagrange strain tensor, and ${}^4\hat{\boldsymbol{C}}_i$ represents the 4th order orthotropic elastic stiffness tensor. After the stress is calculated, it is pushed back to the current configuration and Cauchy stress is obtained. It should be noted that, the deformation gradient in each element $\boldsymbol{F}_i$, is decomposed multiplicatively into elastic and plastic components, where first, a rotation-free plastic deformation $\boldsymbol{F}_{p,i}$ brings the material to an intermediate stress-free configuration and then the elastic deformation $\boldsymbol{F}_{e,i}$ is applied and the material comes to its current configuration.

The plastic rate of deformation is defined in the intermediate configuration as follows:

$$\hat{\boldsymbol{D}}_{p,i} = \mathrm{sym}(\dot{\boldsymbol{F}}_{p,i} \cdot \boldsymbol{F}_{p,i}^{-1}). \tag{3}$$

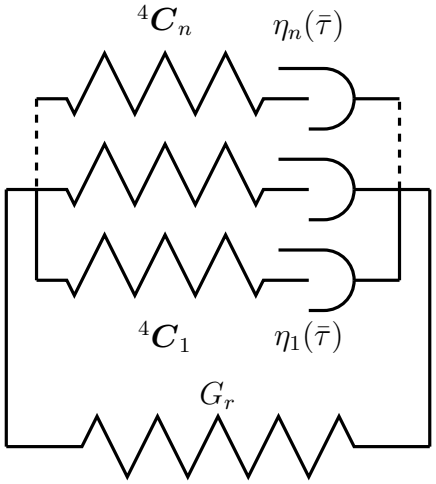

Figure 2: Mechanical analog of the constitutive model consisting of multiple Maxwell elements.

This rate for ith Maxwell element is found through the associated flow rule proposed by van Erp et al. [11]:

$$\hat{\boldsymbol{D}}_{p,i} = \dot{\bar{\gamma}}_{p,i}\hat{\boldsymbol{N}}_i, \tag{4}$$

$$\hat{\boldsymbol{N}}_i = \frac{\partial \bar{\tau}_i}{\partial \hat{\boldsymbol{S}}_{s,i}}, \tag{5}$$

where $\bar{\tau}_i$ is calculated from Hill's effective stress [13] and $\dot{\bar{\gamma}}_{p,i}$ is the equivalent rate of plastic deformation. An Eyring type flow equation [12] is used to find this rate:

$$\dot{\bar{\gamma}}_{p,i} = \frac{\bar{\tau}_i}{\eta_i}, \tag{6}$$

where η_i is the viscosity and is obtained as follows:

$$\eta_i = \eta_{0,i} a(\bar{\tau}), \tag{7}$$

where $\eta_{0,i}$ is the zero shear viscosity, which is modified with the stress shift factor $a(\bar{\tau})$, defined as:

$$a(\bar{\tau}) = \frac{\bar{\tau}/\tau_0}{\sinh(\bar{\tau}/\tau_0)}, \tag{8}$$

where τ_0 is called characteristic stress and $\dot{\gamma}_0$ is the rate constant. It should be noted that the same shift factor is applied to all the branches and the equivalent stress $\bar{\tau}$ in the above equation is calculated from the total driving stress $\boldsymbol{\sigma}_s$ using the Hill's effective stress [13].

For the numerical implementation of the presented model, an implicit scheme is applied. For brevity, the index i, for the ith mode, is eliminated in the following equations. First,

an initial guess is made for the plastic right Cauchy-Green deformation tensor $\boldsymbol{C}_{p_{n+1}}$. Using this value, the plastic right stretch tensor $\boldsymbol{U}_{p_{n+1}}$ is calculated at the end of the time step at t_{n+1}:

$$\boldsymbol{U}_{p_{n+1}} = \sqrt{\boldsymbol{C}_{p_{n+1}}}. \tag{9}$$

Then, the elastic deformation gradient tensor $\boldsymbol{F}_{e_{n+1}}$ is obtained:

$$\boldsymbol{F}_{e_{n+1}} = \boldsymbol{F}_{n+1} \cdot \boldsymbol{U}_{p_{n+1}}^{-1}. \tag{10}$$

Using the elastic deformation gradient tensor $\boldsymbol{F}_{e_{n+1}}$ the driving stress tensor can be calculated from Equation (2). To obtain the stress shift factor a, the equivalent stress $\bar{\tau}_{n+1}$ is obtained from its value at t_n using forward Euler explicit integration. This facilitates the integration process since the stress tensor in each mode can be calculated independent of the other modes at each step:

$$\bar{\tau}_{n+1} = \bar{\tau}_n + \dot{\bar{\tau}}_n \Delta t. \tag{11}$$

After calculating the stress shift factor from Equation (8), the plastic rate of deformation $\hat{\boldsymbol{D}}_{p_{n+1}}$ can be obtained using Equations (4) to (8). In the next step, rate of the plastic right Cauchy-Green deformation tensor $\dot{\boldsymbol{C}}_{p_{n+1}}$ is found as follows:

$$\dot{\boldsymbol{C}}_{p_{n+1}} = 2\boldsymbol{U}_{p_{n+1}} \cdot \hat{\boldsymbol{D}}_{p_{n+1}} \cdot \boldsymbol{U}_{p_{n+1}}. \tag{12}$$

The plastic right Cauchy-Green deformation tensor at the time t_{n+1} is then found according to:

$$\boldsymbol{C}_{p_{n+1}} = \boldsymbol{C}_{p_n} + \Delta t \dot{\boldsymbol{C}}_{p_{n+1}}. \tag{13}$$

This set of equations is solved with the Newton-Raphson scheme. In each iteration of the Newton-Raphson scheme, an initial estimate will be chosen for $\boldsymbol{C}_{p_{n+1}}$ and the residual is obtained by finding the difference between this initial guess and the value calculated from Equation (13). Using the presented implicit integration scheme, the model is implemented in the finite element package ABAQUS as a user material subroutine UMAT.

3 CHARACTERIZATION

Obtaining the input parameters for the proposed constitutive model is discussed in this section. As was explained in the previous section, to obtain the plastic rate of deformation tensor $\hat{\boldsymbol{D}}_p$, Hill's effective stress and an Eyring flow equation is used. One of the kinetics parameters that need to be determined is the characteristic stress τ_0, which determines the slope of yield stress vs. logarithm of strain rate [3]. Because the effects of the loading rate and material orientation are factorizable, this value is the same for all the orientations. Figure 3 (a), shows yield stress vs. logarithm of strain rate for orientation of $\phi = 90°$. By fitting the Eyring equation (Equation (6)) to this data, the value for τ_0 is obtained (Table 1). Plastic anisotropy parameters such as R_{11} and R_{12} are required for calculation of Hill's

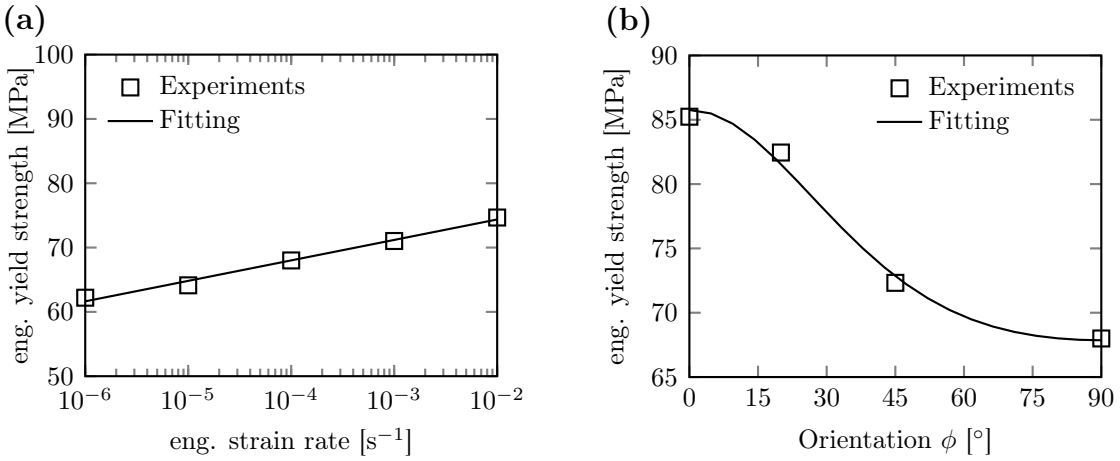

Figure 3: (a) Measured value for yield strength at (a) different rates for the reference orientation of $\phi = 90°$ and at (b) different orientations at a strain rate of 10^{-4} s^{-1}.

Table 1: Model parameters.

characteristic stress	Hill parameters		
τ_0 [MPa]	R_{11}	R_{22}	R_{12}
0.8	1.26	1	1.1

effective stress [11]. The parameter R_{11}, shows the ratio of yield in 1 direction, which here is taken as the main direction of mold flow ($\phi = 0°$) which has the most amount of fiber alignment, to yield in the reference direction. The reference yield direction is chosen as the direction perpendicular to the main mold flow direction ($\phi = 90°$), which has the least amount of fiber alignment, hence $R_{22} = 1$. The value for R_{12} shows, the ratio of shear stress in 12 direction to the reference shear stress. Because of the factorizable behavior shown in the previous section, the values for R_{11}, R_{22} and R_{12} are independent of the strain rate. In Figure 3 (b), Hill function is fitted to yield strength values measured for different orientations at strain rate of 10^{-4} s^{-1}. The obtained values for different Hill parameters are shown in Table 1.

For obtaining the moduli and viscosity for each mode (Figure 2), a procedure similar to [14] is followed. The procedure proposed in [14] is for the isotropic case. The method is extended to the orthotropic response, by first finding the moduli in a reference direction by the same procedure proposed in [14] and then, assuming the same distribution of the elastic parameters between different modes as the reference direction. Here, the direction $\phi = 90°$ is chosen as the reference direction and therefore E_{22} is found for different modes. The obtained values for E_{22} and also viscosities and relaxation times are shown in Table 2. Total values for different elastic parameters are also found from the stress-strain curves for different orientations and shown in Table 3. Sum of E_{22} values for different modes is

Table 2: Normal relaxation times, moduli and zero shear viscosities, fitted using using measurements at $\phi = 90^\circ$ and $\dot{\varepsilon} = 10^{-4}$ s^{-1}.

Mode	$\lambda_i^{norm.}$[s]	$E_{22,i}$[MPa]	$\eta_{0,i}$[MPa s]
1	2.07×10^{22}	1659	1.14×10^{25}
2	1.81×10^{21}	164	9.91×10^{22}
3	2.07×10^{20}	136	9.39×10^{21}
4	2.37×10^{19}	118	9.36×10^{20}
5	2.71×10^{18}	93	8.40×10^{19}
6	3.10×10^{17}	83	8.61×10^{18}
7	3.54×10^{16}	71	8.43×10^{17}
8	4.05×10^{15}	65	8.76×10^{16}
9	4.63×10^{14}	56	8.65×10^{15}
10	5.29×10^{13}	57	9.99×10^{14}
11	6.04×10^{12}	49	9.81×10^{13}
12	6.91×10^{11}	47	1.09×10^{13}
13	7.90×10^{10}	42	1.10×10^{12}
14	9.03×10^{9}	43	1.30×10^{11}
15	1.03×10^{9}	37	1.27×10^{10}
16	1.18×10^{8}	36	1.41×10^{9}
17	1.35×10^{7}	36	1.62×10^{8}
18	1.54×10^{6}	27	1.40×10^{7}
19	1.76×10^{5}	39	2.31×10^{6}
20	2.01×10^{4}	28	1.86×10^{5}
21	2.30×10^{3}	25	1.89×10^{4}
22	2.63×10^{2}	44	3.84×10^{3}
23	3.01×10^{1}	59	5.91×10^{2}

Table 3: Elastic parameters of the model.

E_{11} [MPa]	E_{22} [MPa]	G_{12} [MPa]	$\nu_{12} = \nu_{23}$
4181	2988	1184	0.26

approximately equal to the total E_{22} value shown in Table 3. A dimensionless vector m can be found according to:

$$\begin{aligned} E_{22} &= \sum_{i=1}^{n} E_{22,i} = \sum_{i=1}^{n} m_i E_{22}, \\ \sum_{i=1}^{n} m_i &= 1. \end{aligned} \tag{14}$$

Then using the assumption of the same distribution of elastic properties, one can write:

$$^4\boldsymbol{C}_i = m_i \, ^4\boldsymbol{C}. \tag{15}$$

It should be noted that values of Poisson ratio are assumed to be the same for all the modes.

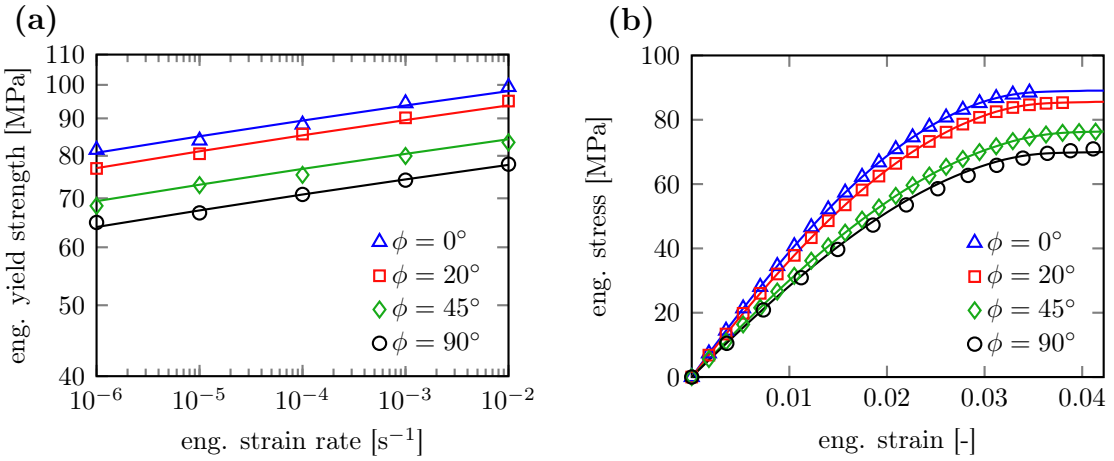

Figure 4: Model predictions (solid lines) and test results (markers) for (a) yield strength at various material orientations and strain rates and (b) stress-strain curves at different material orientations at a strain rate of $\dot{\varepsilon} = 10^{-4}$ s^{-1}.

4 RESULTS AND DISCUSSION

The presented constitutive model is implemented as an ABAQUS user material subroutine using the implicit scheme presented in section 2. After finding the material parameters following the procedure presented in the previous section, uniaxial tension tests are simulated in ABAQUS. As was discussed in the previous section, uniaxial test results at $\phi = 90°$ for different strain rates and also results at a strain rate of 10^{-4} s^{-1} for different orientations were used to find the model parameters. Values for yield stress for other orientations and strain rates are obtained from ABAQUS simulations and are compared to the experimental measurements in Figure 4 (a). In Figure 4 (b), stress-strain curves from ABAQUS simulations are compared with the test results. As can be seen in Figure 4, there is a good match between the model predictions and experimental data for yield strength, and with the use of a spectrum of relaxation times, the model is able to capture the nonlinear pre-yield response with good accuracy.

Figure 5 (a) shows the results for creep simulations. Applied stress is plotted vs. time-to-failure and model predictions (solid lines) are compared with the experimental data (markers). Figure 5 (b) shows strain evolution in time for different stress values from finite element simulations. The failure is considered as the point where plastic localization happens and a very high strain rate is observed. Failure points are shown with the markers in this figure.

The comparison of the model predictions and the experiments shows the capabilities of the model in predicting both the yield and pre-yield behavior. The rate-dependence and anisotropic response are modeled with good accuracy. The factorizable dependence of the yield stress on loading rate and material orientation is also captured.

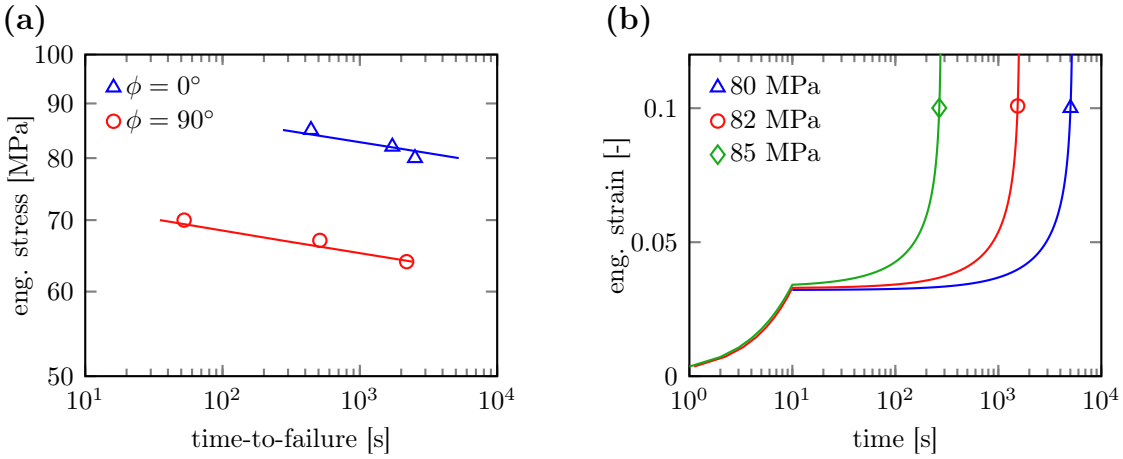

Figure 5: (a) Comparison of model predictions (solid lines) and experimental measurements (markers) for time-to-failure at different stress levels; (b) evolution of engineering strain with time in creep simulations for $\phi = 0°$ with different stress values (markers indicate the failure points).

5 CONCLUSIONS

In this paper, an anisotropic viscoelastic-viscoplastic macro-mechanical model was proposed for short-fiber reinforced thermoplastics. Results for uniaxial tension tests at different strain rates and orientations were presented and it was shown that the effect of strain rate and material orientation on the yield are factorizable. Hill's effective stress and an Eyring type flow equation were used to model the rate-dependent and anisotropic yield behavior. The nonlinear, anisotropic and rate-dependent pre-yield regime was modeled with application of a spectrum of relaxation times and orthotropic springs in each Maxwell element. An implicit scheme was presented for the integration of the constitutive model. It was shown that by use of the factorizability feature, the effects of strain rate and orientation on the yield can be taken apart in the characterization process. An effective method for finding moduli and relaxation times for different modes was also presented. The model predictions for constant strain rate and creep tests were compared with experiments and it was shown that a good agreement exists between the results.

REFERENCES

[1] L.E. Govaert, P.H.M. Timmermans, and W.A.M. Brekelmans. The influence of intrinsic strain softening on strain localization in polycarbonate: modeling and experimental validation. *Journal of Engineering Materials and Technology*, 122(2):177–185, 2000.

[2] T.A. Tervoort, E.T.J. Klompen, and L.E. Govaert. A multi-mode approach to finite, three-dimensional, nonlinear viscoelastic behavior of polymer glasses. *Journal of Rheology*, 40(5):779–797, 1996.

[3] E.T.J. Klompen, T.A.P. Engels, L.E. Govaert, and H.E.H. Meijer. Modeling of the postyield response of glassy polymers: influence of thermomechanical history. *Macromolecules*, 38(16):6997–7008, 2005.

[4] R.N. Haward and G. Thackray. The use of a mathematical model to describe isothermal stress-strain curves in glassy thermoplastics. In *Proc. R. Soc. Lond. A*, volume 302, pages 453–472. The Royal Society, 1968.

[5] M.C. Boyce, D.M. Parks, and A.S. Argon. Large inelastic deformation of glassy polymers. part i: rate dependent constitutive model. *Mechanics of Materials*, 7(1):15–33, 1988.

[6] E.M. Arruda and M.C. Boyce. Evolution of plastic anisotropy in amorphous polymers during finite straining. *International Journal of Plasticity*, 9(6):697–720, 1993.

[7] O.A. Hasan, M.C. Boyce, X.S. Li, and S. Berko. An investigation of the yield and postyield behavior and corresponding structure of poly (methyl methacrylate). *Journal of polymer science part B: polymer physics*, 31(2):185–197, 1993.

[8] C.P. Buckley and D.C. Jones. Glass-rubber constitutive model for amorphous polymers near the glass transition. *Polymer*, 36(17):3301–3312, 1995.

[9] C.P. Buckley, P.J. Dooling, J. Harding, and C. Ruiz. Deformation of thermosetting resins at impact rates of strain. part 2: constitutive model with rejuvenation. *Journal of the Mechanics and Physics of Solids*, 52(10):2355–2377, 2004.

[10] J.J. Wu and C.P. Buckley. Plastic deformation of glassy polystyrene: a unified model of yield and the role of chain length. *Journal of Polymer Science Part B: Polymer Physics*, 42(11):2027–2040, 2004.

[11] T.B. van Erp, C.T. Reynolds, T. Peijs, J.A.W. van Dommelen, and L.E. Govaert. Prediction of yield and long-term failure of oriented polypropylene: Kinetics and anisotropy. *Journal of Polymer Science Part B: Polymer Physics*, 47(20):2026–2035, 2009.

[12] T.A. Tervoort, R.J.M. Smit, W.A.M. Brekelmans, and L.E. Govaert. A constitutive equation for the elasto-viscoplastic deformation of glassy polymers. *Mechanics of Time-Dependent Materials*, 1(3):269–291, 1997.

[13] R. Hill and E. Orowan. A theory of the yielding and plastic flow of anisotropic metals. *Proceedings of the Royal Society of London. Series A. Mathematical and Physical Sciences*, 193(1033):281–297, 1948.

[14] L.C.A. van Breemen, E.T.J. Klompen, L.E. Govaert, and H.E.H. Meijer. Extending the egp constitutive model for polymer glasses to multiple relaxation times. *Journal of the Mechanics and Physics of Solids*, 59(10):2191–2207, 2011.